Integrated B1+ Mapping for Hyperpolarized 13C MRI in a Clinical Setup using Multi-Channel Receive Arrays

Hansen, Rie Beck; Shin, Peter J.; Gordon, Jeremy W.; van Criekinge, Mark; Carvajal, Lucas; Hanson, Lars G. ; Ardenkjær-Larsen, Jan Henrik; Vigneron, Daniel B.

Publication date:
2018

Document Version
Publisher's PDF, also known as Version of record

3698

Integrated B1+ Mapping for Hyperpolarized 13C MRI in a Clinical Setup using Multi-Channel Receive Arrays

Rie B Hansen[1], Peter J Shin[2], Jeremy W Gordon[2], Mark Van Criekinge[2], Lucas Carvajal[2], Lars G Hanson[1], Jan H Ardenkjær-Larsen[1], and Daniel B Vigneron[2]

[1]Department of Electrical Engineering, Technical University of Denmark, Kgs. Lyngby, Denmark, [2]Department of Radiology and Biomedical Imaging, UCSF, San Francisco, CA, United States

Synopsis

For hyperpolarized ^{13}C MRI acquisitions aimed at metabolic rate constant estimation, the Bloch-Siegert shift enables encoding of the transmit field (B_1^+-field) amplitude within a single hyperpolarized substrate injection. This ability is needed since most clinical hyperpolarized MRI studies use inhomogeneous transmit coils, and because kinetic modeling based on incorrect flip angles can lead to incorrect rate constant estimations. This study demonstrates the feasibility of integrated B_1^+ mapping for large volume thermal and hyperpolarized phantoms in a clinical setup using a clamshell transmit coil and a 16-channel receive array, and a 3D stack-of-spirals sequence. Phase-sensitive coil-combination was achieved using ESPIRiT.

Introduction

By means of the Bloch-Siegert shift, the transmit field (B_1^+) amplitude can be encoded into the signal phase during MRI acquisition.[1] For hyperpolarized carbon-13 MRI, this can provide data that enable B_1^+-field mapping together with spatial mapping of metabolic rate constants within one hyperpolarized substrate injection.[2] Integrated B_1^+ mapping is motivated by an extensive use of inhomogeneous clamshell-type transmit coils[3] in clinical hyperpolarized MRI applications,[4–6] together with reduced quantitation accuracy of rate constants when modeling with incorrect flip angles.[7] While proof-of-principle integration of Bloch-Siegert B_1^+ mapping in a hyperpolarized study has been shown,[2] this study focuses on a clinical setup using multi-channel arrays that enable parallel imaging for acquisition acceleration. However, for phase-based B_1^+ mapping methods, phase-sensitive coil-combination is a challenge. By using ESPIRiT[8] for coil-combination, SNR-levels comparable to using sum-of-squares can be achieved, while preserving phase information.

Methods

Bloch-Siegert B_1^+ mapping was integrated in a 3D stack-of-spirals sequence with singleband spectral-spatial (SPSP) excitation. By alternating between positive and negative off-resonance Bloch-Siegert pulses through the full dynamic acquisition, B_1^+ mapping is possible across multiple time points. This makes the method robust against spatially varying signal support over time; expected in vivo.

All data were acquired on an MR750 3T scanner (GE Healthcare, Waukesha, WI, USA) with a ^{13}C clamshell coil for excitation and a 16-channel coil for reception (Rapid Biomedical, Rimpar, Germany). See coil setup in Figure 1.

Multi-compartment thermal phantom: Image data were acquired for a 32x32x12 cm^3 FOV with a 30-ms single-shot-spiral readout in the axial plane and 10 phase-encodes (superior/inferior). Two measurements were conducted with 4-ms Bloch-Siegert pulses applied +/-2 kHz off-resonance. Other scan parameters: TR 1 s; flip angle 70°; NEX 32; SPSP frequencies four (Ethylene Glycol, Urea, Alanine, Acetate (Δf = [0,3177,3598,3803] Hz)). The spirals were gridded to a 54x54 matrix and filtered to result in an isotropic resolution of 1.2 cm. The data were coil-combined using ESPIRiT for each 3D volume, across frequencies and time points, before estimating B_1^+ maps as previously described.[1]

Hyperpolarized [1-^{13}C]pyruvate phantom: 1.47 g of [1-^{13}C]pyruvic acid doped with 15 mM electron paramagnetic agent was polarized for 3 hours in a 5T Spinlab at 0.78 K. The sample was rapidly dissolved and neutralized yielding 42 mL pyruvate (259 mM, 44 % polarization). This was added to a sphere containing ~2.5 L water. Imaging started 43 s after injection. The sequence was run three times with 16 time points for each run and a 20-s and 10-s delay between runs. Other scan parameters: TR 200 ms; flip angle 5°. FOV, spiral, Bloch-Siegert pulse, and reconstruction method were identical to those for the thermal phantom experiment. Due to long relaxation times and the short TR, the measured signal depends critically on T_1, T_2, B_1 and B_0, so fitting of the measured signal to a signal equation was not attempted. This could have provided validation for the B_1^+ maps.

Results and Discussion

Figure 2(b-c) illustrate how coil-combination by ESPIRiT results in similar or higher SNR levels compared to sum-of-squares reconstruction. Figure 3 shows the B_1^+ mapping results together with a simulated B_1^+-field for the clamshell transmitter. All maps show the same pattern. The slightly smaller inhomogeneity of the simulated map compared to the Bloch-Siegert maps is likely explained by a geometry symmetry assumption for the simulation, while the B_1^+ field of the clamshell coil has experimentally been shown to be asymmetric as visible in Figure 3(a).

Figure 4 shows 24 B_1^+ maps extracted from the 24 pairs of consecutive time points of the hyperpolarized experiment. Ideally these would be identical, but as SNR decreases so does reliability of B_1^+ mapping. In the higher SNR region, flip angles were estimated consistently up to 100 s after acquisition start (70 s active scan time), while in low SNR regions estimates became less consistent after 40 s active scan time. A minimum SNR of ~40 is needed for accurate B_1^+ estimation. Figure 5 shows scatter plots for the voxel-wise relative flip angle values across experiments. A higher linear correlation was observed for high relative flip angle voxels compared to voxels with low relative flip angle; as these voxels also had low SNR, this is not unexpected.

Conclusion

This study demonstrated feasibility of integrated B_1^+ mapping for a clinical hyperpolarized ^{13}C coil setup, by means of the Bloch-Siegert shift and ESPIRiT for coil-combination. Future studies should optimize the Bloch-Siegert pulse design to avoid SAR issues, test integration of B_1^+ mapping in other sequences, validate the results in vivo, and test integrated B_1^+ mapping with parallel imaging to fully utilize multi-channel receive coils.

Acknowledgements

This work has been partly funded by the Independent Research Fund Denmark (DFF – 4005-00531), the Danish National Research Foundation (DNRF124), and the Elite Research travel grant (6161-00043B).

References

1. Sacolick, L. I., Wiesinger, F., Hancu, I. & Vogel, M. W. B1 mapping by Bloch-Siegert shift. *Magn. Reson. Med.* **63**, 1315–1322 (2010).

2. Lau, A. Z., Chen, A. P. & Cunningham, C. H. Integrated Bloch-Siegert B1 mapping and multislice imaging of hyperpolarized 13C pyruvate and bicarbonate in the heart. *Magn. Reson. Med.* **67**, 62–71 (2012).

3. Tropp, J. *et al.* Multi-channel metabolic imaging, with SENSE reconstruction, of hyperpolarized [1-13C] pyruvate in a live rat at 3.0 tesla on a clinical MR scanner. *J. Magn. Reson.* **208**, 171–177 (2011).

4. Cunningham, C. H. *et al.* Hyperpolarized 13C Metabolic MRI of the Human Heart: Initial Experience. *Circ. Res.* **119**, 1177–1182 (2016).

5. Park, I. *et al.* Dynamic Hyperpolarized 13C Metabolic Imaging of Patients with Brain Tumors. in *Proc. Intl. Soc. Mag. Reson. Med.* 555 (2017).

6. Gordon, J. W. *et al.* Human Hyperpolarized C-13 MRI Using a Novel Echo-Planar Imaging (EPI) Approach. in Proc. Intl. Soc. Mag. Reson. Med. 728 (2017).

7. Chen, H.-Y. *et al.* Phase II Clinical Hyperpolarized 13C 3D-Dynamic Metabolic Imaging of Prostate Cancer using a B1-insensitive Variable Flip Angle Design. in *Proc. Intl. Soc. Mag. Reson. Med.* 725 (2017).

8. Uecker, M. *et al.* ESPIRiT - An eigenvalue approach to autocalibrating parallel MRI: Where SENSE meets GRAPPA. *Magn. Reson. Med.* **71**, 990–1001 (2014).

Figures

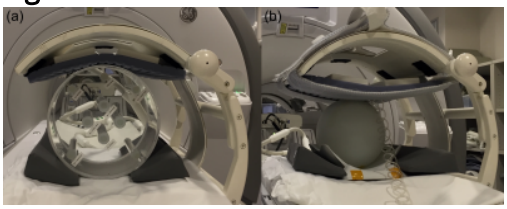

Figure 1: Coil setup for (a) the thermally polarized phantom experiment, and (b) the hyperpolarized phantom experiment. The pictures show the clamshell coil and the top paddle of the 16-channel receive array. The bottom paddle is under the linen. The phantom in (a) is a 20-cm long cylinder with 24 cm inner diameter and eight cylindrical compartments. Six of these are filled with 1.5 M [1-^{13}C]-L-Alanine, 2.0 M ^{13}C-Urea, and 2.0 M Sodium [1-^{13}C]Acetate, respectively, the last two are empty. The large compartment contains natural abundance Ethylene Glycol. The phantom in (b) is a sphere with 18 cm diameter.

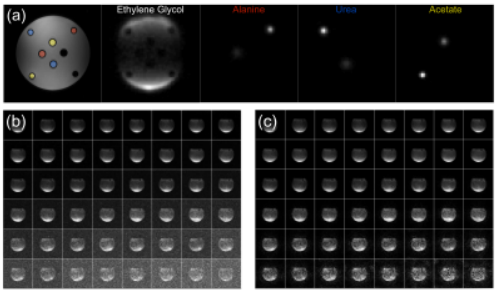

Figure 2: (a) Proton reference and magnitude image results from the thermal phantom experiment (summed over slices and over time). The colors on the reference image indicate the compartment contents, i.e. red for [1-^{13}C]-L-Alanine, blue for ^{13}C-Urea, and yellow for Sodium [1-^{13}C]Acetate. (b-c) Individually scaled magnitude images from the hyperpolarized phantom experiment for the center slice (8x6 time points shown left to right, row-by-row). The images result from coil-combination using (b) sum-of-squares reconstruction and (c) ESPIRiT.

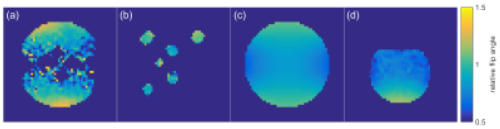

Figure 3: B_1^+ mapping results for the thermal phantom experiment (a-b), and for the hyperpolarized phantom experiment (d). (a) shows the map estimated from the Ethylene Glycol images, while (b) shows the combined maps from the Alanine, Urea and Acetate images. (c) shows the simulated B_1^+-field variation. All maps shown are based on the center-slice. Notice that because of normal spatial point spread, the estimated B_1^+ maps for the thermal phantom in (a-b) exceed the compartment borders in high SNR regions. This explains why the outer signal voids for the Ethylene Glycol compartment in (a) are hardly noticeable.

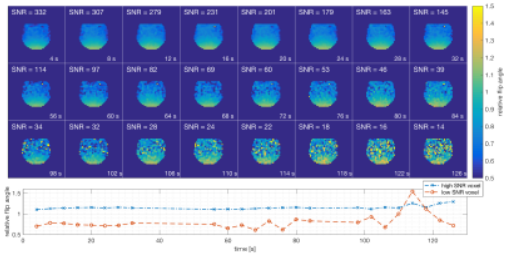

Figure 4: B_1^+ mapping results for the center-slice across the full dynamic acquisition of the hyperpolarized phantom. Peak SNR values were estimated based on the maximum absolute signal divided by the standard deviation of the real part of the noise. The first map is based on two images acquired after 4 s, while the last map is based on two images acquired after 126 s. The bottom graph shows estimated relative flip angle values for two different voxels, a high and a low SNR voxel, across time points.

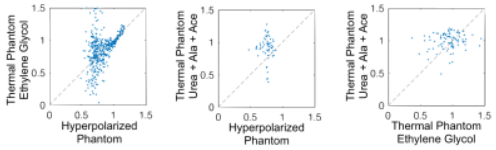

Figure 5: Scatter plots of voxel-wise estimations of relative flip angle across experiments. The dashed lines indicate a linear correlation of 1. Ala = Alanine, Ace = Acetate. Coil loading across experiments is assumed to be similar.

Proc. Intl. Soc. Mag. Reson. Med. 26 (2018)
3698